A new method for calculating laser intensity distribution on workpiece surface in laser directed energy deposition process by considering powder stream distribution and laser attenuation

Niloufar Sobhanieh[1], Javad Akbari[1,*], Mahmoud Moradi[2]

[1]School of Mechanical Engineering, Sharif University of Technology, Tehran, Iran

[2]School of Mechanical, Aerospace and Automotive Engineering, Faculty of Engineering, Environment and Computing, Coventry University, Gulson Road, Coventry, CV1 2JH, United Kingdom.

*Corresponding E-mail: Akbari@sharif.edu

Abstract

Laser-directed energy deposition is a fast-growing method for manufacturing complex geometries and materials that are hard to shape with conventional manufacturing methods. However, there are some aspects of this process that need more researches and experiments to be completely understood. One of these is laser attenuation and laser intensity distribution on the workpiece surface. In this paper, a new method is proposed for calculating laser attenuation without simplification applied in previous works. Despite other studies that consider a predefined powder distribution, the result of a developed 3D CFD model of the powder stream is utilized for defining the position of particles in the powder stream. The divergence and spatial distribution of the laser beam are considered by dividing the laser beam in a radial direction. A GUI has been developed in MATLAB to take CFD model output as input for calculating laser attenuation with Beer-Lambert law and plotting the laser intensity on the workpiece surface after being attenuated. The influence of powder mass flow rate, powder size, and workpiece position on laser attenuation and its intensity distribution is investigated. It is shown that increase in powder flow rate would increase laser attenuation almost linearly. It has also indicated that smaller particles would attenuate more energy than larger ones while the powder mass flow rate is kept constant. More specifically, decreasing powder size from 100 μ to 20 μ, increases attenuation from 18% up to 55%. The size of powder particles affects powder stream distribution and consequently, this affects the laser intensity profile on the workpiece surface. The result of investigating the workpiece position shows that the position of the workpiece influences the laser attenuation, powder catchment, and maximum intensity of laser energy.

Keywords: Laser Directed Energy Deposition, Gas-Powder model, Laser attenuation, Laser energy distribution

1. Introduction

Laser Directed Energy Deposition (LDED) is an additive manufacturing process which is attaining so many interests recently. Parts with complex geometry and with materials that are hard to shape by conventional manufacturing methods can be made by LDED [1-8]. In this process, a laser beam melts the workpiece surface and makes a melt pool in which the injected powders from a nozzle, fall into and melt. By the laser beam passing the melt pool, it cools and solidifies to form a layer[9](Fig. 1).

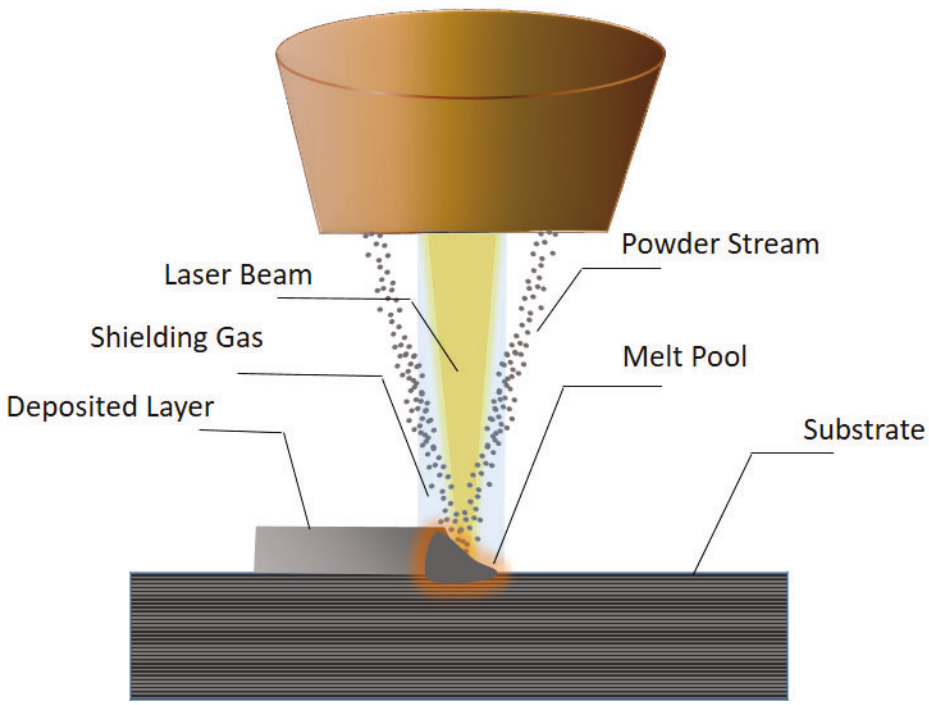

Fig. 1 Schematic of LDED process

There are many studies investigating LDED process experimentally or computationally from various aspects. Despite all the studies on this process, there are so many aspects of it that are not completely known to us. One of the most effective parameters on the process and quality of the final part is the laser beam energy and its intensity distribution on the workpiece[10-15]. Insufficient heat input may cause ineffective melt of substrate surface and powders, which may cause lack of fusion and failure of the process or poor quality of the manufactured part[16, 17]. On the other hand, high energy can induce powders' evaporation[18-20]. So it is

important to know that how much energy and with what distribution is delivered to the surface and the melt pool. It should be considered that some of the laser energy becomes extinct as the laser beam passes through the powder's cloud. Thus, the amount of energy reaching the workpiece surface is not equal to the initial energy that was set on the machine. The amount of laser energy extinct by the powders is called “laser energy attenuation”. Laser energy attenuation is of great importance and it could not be ignored, as Lin[21] indicated in his study, more than 50% of the laser energy could be lost in the interaction of laser beam with powder stream. The powder stream distribution has great impact on laser energy attenuation and subsequently on the energy flux to the melt pool [22, 23]. Zhang et al. [24] investigated the effect of nozzle dimension on powder stream structure by the use of computational fluid dynamics (CFD) and showed that this distribution is dependent on the nozzle dimension. Liu et al. [25] studied the effect of both geometries and process parameters on powder flow distribution. Guan et al. [26] simulated spatial distribution of the flying powder particles by combining CFD and discrete element methods. Kovalev et al. [27] modeled the transportation of powder during LDED process and investigated particle trajectories for various nozzles.

Despite the importance of powder flow distribution, most of the studies on laser energy, tried to calculate laser attenuation by implementing simplifications on the powder stream structure and used Gaussian or other pre-determined distribution. There are also some simplifying assumptions on the shape of the laser beam, the way laser beam, and powders interact, and the method of calculating laser attenuation. Diniz Neto[28] calculated laser attenuation in laser surface processing by assuming the laser beam as a cylinder of the constant radius with Gaussian spatial distribution. In this study, the particles of the powder jet from a lateral nozzle were treated as originating from a point source and traveling at a constant velocity. In his other study [29] he considered the divergence of the laser beam but still assumed two density

distributions for the powder stream, Gaussian and varying with the inverse of the square of the distance. Pinkerton [30]proposed a laser attenuation model based on the shadow model. He considered that, at each position in t the powder concentration distribution across a stream centerline is Gaussian and ignored the effect of drag and gravity on the powder stream. Tabernero et al. [31] also presented a laser attenuation model based on the shadow model. It was considered that attenuation in laser cladding, with an annular nozzle, is produced only after the consolidation plane of the annular powder stream and assumed that the powder concentration distribution is Gaussian after this plane. This study revealed that smaller particles cause more attenuation while other parameters in the process are constant. Wu et al. [32] investigated the effects of beam profiles on laser attenuation by assuming that all powder particles injected from a discontinuous coaxial nozzle have the same magnitude of velocity when they leave the nozzle exit and their trajectory is a line. He also considered the powder stream from each of the four nozzles has Gaussian distribution. Deves[33] has done one of the most accurate studies on calculating laser attenuation during laser cladding with an annular nozzle. He utilized the ray-tracing method and studied the effect of powder flow profile on the laser energy distribution that reaches the workpiece surface. This is despite all other literature that proposed statistical distributions for powder stream and did not take into account the complex powder flow profile that is present in a practical system. It was a complicated and time-consuming method and did not investigate the influence of the position of the workpiece and laser focal plane on attenuation.

In this paper, a new method is proposed for the calculation of laser attenuation in laser directed energy deposition process without simplification in laser beam properties and powder stream distribution. The divergence of the laser beam and its energy density distribution is being considered by partitioning the laser beam in the

radial direction. A powder flow model is developed in ANSYS Fluent to define powder particles' position. A GUI has been created in MATLAB to get the 3D powder flow model result as input for the calculation of laser energy attenuation. The influence of powder size, powder feed rate, and position of the workpiece on laser attenuation and intensity distribution on the workpiece is investigated.

2. Gas-Powder Flow Model

In the LDED process, powder particles are usually carried by argon gas. So, the powder trajectory could be solved using the discrete phase model (DPM) available in ANSYS FLUENT software, In this software the gas is treated as a continuum and the powder is simulated as discrete phase dispersing in the continuous argon gas phase[19, 23].

2.1. Modeling of Gas-phase

The gas-powder flow is characterized by turbulence and described by the standard $k-\varepsilon$ model which is the most popular turbulence model in practical use. The turbulent kinetic energy k, and the viscous dissipation rate of turbulent kinetic energy ε , characterize the turbulent filed. This model includes continuity equation of mass, momentum conservation equations, and $k-\varepsilon$ kinetic energy equations. The governing equations are[34-36]:

Continuity equation:

$$\frac{\partial \bar{u}_i}{\partial x_i} = 0 \tag{1}$$

Conservation of mean momentum (Navier-Stokes):

$$\frac{\partial}{\partial x_i}\left(\rho \bar{u}_j \bar{u}_i\right) + \frac{\partial}{\partial x_j}\left(\rho \bar{u}'_i \bar{u}'_i\right) = -\frac{\partial \bar{p}}{\partial x_i} + \frac{\partial}{\partial x_i}\left[\mu\left(\frac{\partial \bar{u}_i}{\partial x_j} + \frac{\partial \bar{u}_j}{\partial x_i}\right)\right] \tag{2}$$

where $i.j = 1.2.3.\bar{u}_i$ is the mean velocity vector in the ith direction, p is the pressure, μ is the dynamic viscosity, ρ is the density and $\rho \bar{u}'_i \bar{u}'_i$ is the Reynolds stress.

Conservation of the kinetic energy of turbulence:

$$\frac{\partial}{\partial x_j}(\rho \bar{u}_j k) = \frac{\partial}{\partial x_j}\left(\frac{\mu_t}{\sigma_k}\frac{\partial k}{\partial x_j}\right) + G_k + G_b - \rho\varepsilon \quad (3)$$

Conservation of the dissipation of kinetic energy of turbulence:

$$\frac{\partial}{\partial x_j}(\rho \bar{u}_j \varepsilon) = \frac{\partial}{\partial x_j}\left(\frac{\mu_t}{\sigma_\varepsilon}\frac{\partial \varepsilon}{\partial x_j}\right) + C_1\frac{\varepsilon}{k}(G_k + G_b) - C_2\rho\frac{\varepsilon^2}{k} \quad (4)$$

$$G_k = \mu_t \frac{\partial \bar{u}_i}{\partial x_j}\left(\frac{\partial \bar{u}_i}{\partial x_j} + \frac{\partial \bar{u}_j}{\partial x_i}\right) \quad (5)$$

$$G_b = -g_i \frac{\mu_t}{Pr_t}\frac{\partial \rho}{\partial x_i} \quad (6)$$

where $i.j = 1.2.3.\mu = \mu_0 + \mu_t$, ($\mu_0$- molecular viscosity, μ_t- turbulent viscosity), and Pr_t is the turbulent Prandtl number of energy. $C_1.C_2.\sigma_k$ and σ_ε have the following default values[37, 38]. These default values have been determined for fundamental turbulent flows including frequently encountered shear flows like boundary layers, mixing layers, and jets as well as for decaying isotropic grid turbulence[37, 39].

$$C_1 = 1.44; C_2 = 1.92; \sigma_k = 1.0;\ \sigma_\varepsilon = 1.30 \quad (7)$$

2.2. Modeling of powder flow

The trajectory of the discrete phase of a particle is solved by integrating the force balance on the particle in a Lagrangian reference frame. By considering drag and gravity force, governing equation on the motion of each particle with density ρ_p and diameter d_p is as[34, 35]:

$$\frac{du_i^p}{dt} = \frac{18\mu}{\rho_p d_p^2}\frac{C_D Re}{24}\left(u_i - u_i^p\right) + \frac{\rho_p - \rho}{\rho_p} g_i \quad (8)$$

where $i = 1.2.3.\ u_i^p$ is the particle velocity, and u_i is the velocity of the carrier phase. μ is the fluid phase dynamic viscosity and Re is Reynolds number and C_D is the drag coefficient.

2.3. Gas-powder flow simulation results

In order to simulate the gas-powder stream, without laser radiation, as it is shown in ***Fig. 2***, a 3D model of the turbulent gas-powder flow-based on the nozzle setup, has been developed in ANSYS FLUENT software.

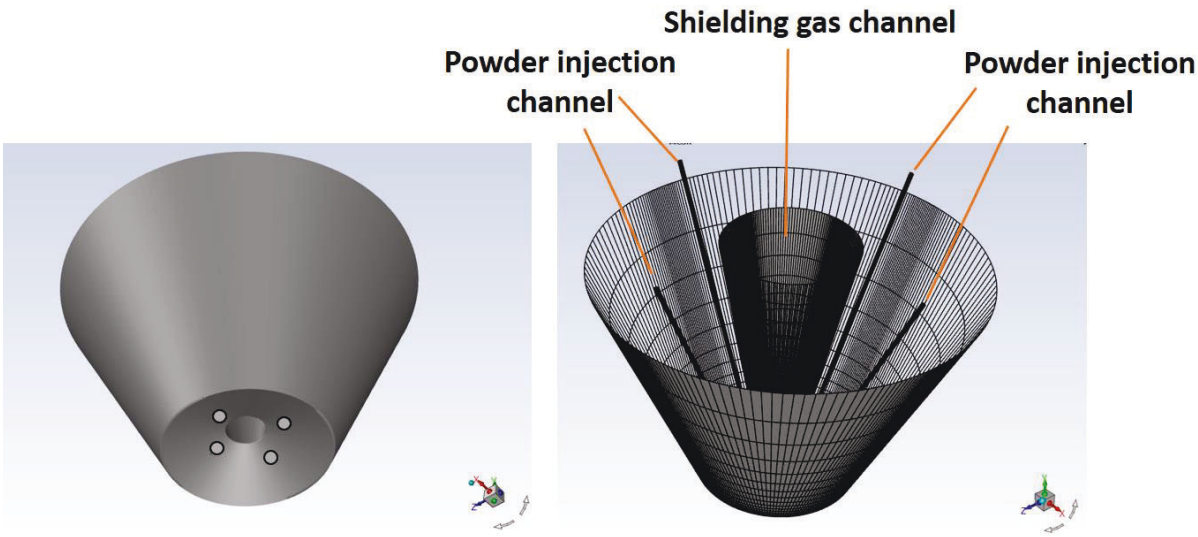

Fig. 2. 3D model of nozzle. Left: Bottom view, Right: Top view

The nozzle setup is based on the setup used in experimental study done by Moradi [40, 41]. As shown in **Fig. 3** the brass nozzle has four annular channels which are designed to focus the powder particles in the powder concentration plane. The argon shielding gas is flowing through the axial channel.

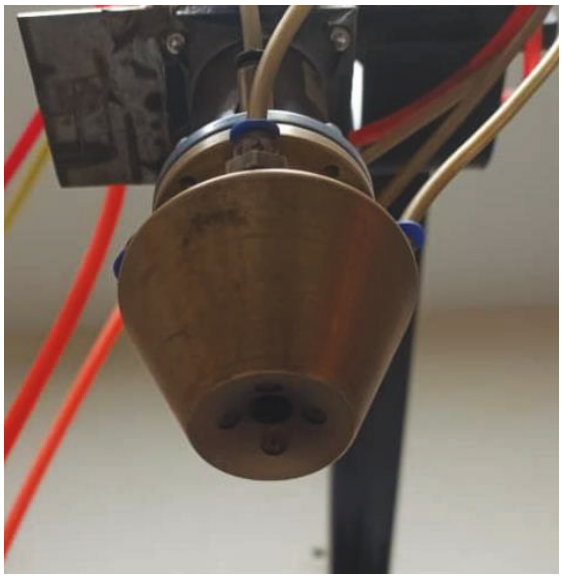

Fig. 3. Nozzle setup in Moradi study[40, 41]

The geometric domain and boundary condition for simulated gas-powder flow is shown in **Fig. 4**.

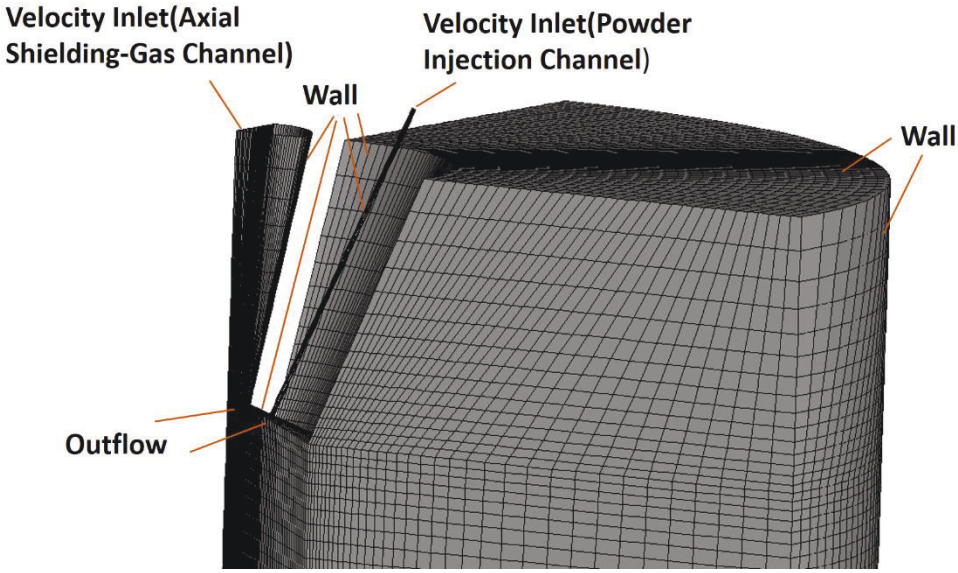

Fig. 4. geometric domain and boundary condition for simulated gas-powder flow

The simulation is applied on experimental setting of Moradi[41] study to verify the result of modeling. The particles with an average size of 23 μm with a density of 8 gr/cm^3 and 20 g/min mass flow rate were injected to the nozzle inlet. The coaxial gas flow rate and annular gas flow rates are 3 and 6 lit/min. As shown in **Fig. 5** , the

simulation result for the position of the concentration plane of powder flow is in good agreement with the experimental results.

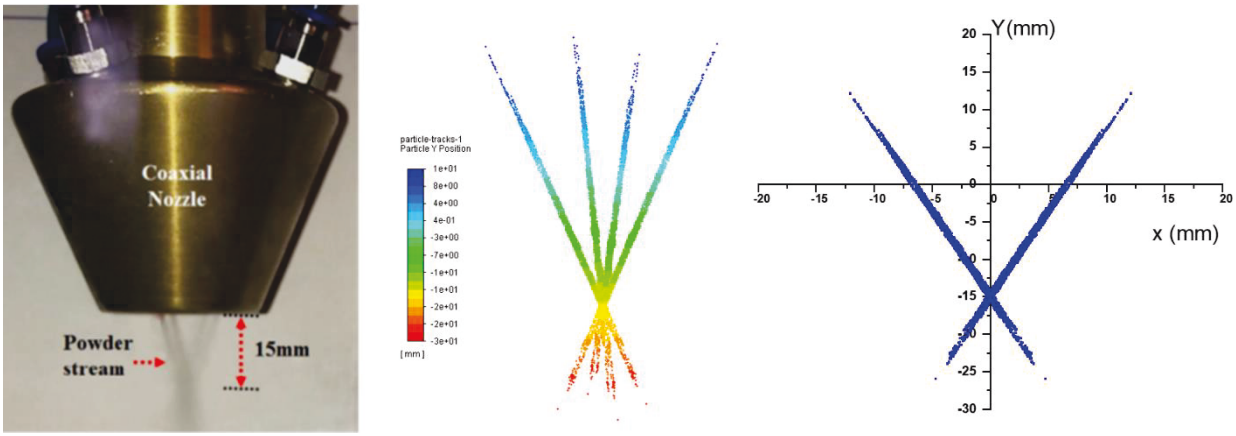

Fig. 5. Left: powder flow and concentration plane position in Moradi's[40] Study; Middle: powder flow in 3D simulation in ANSYS FLUENT software, Right: Particles' position in powder flow from 3D simulation in ANSYS Fluent software

3. Laser Attenuation

For calculating laser attenuation, a Gaussian spatial distribution of radiation intensity is assumed for the laser beam, the intensity being given by[22]:

$$\boldsymbol{I(x.y.z) = \frac{2P_0}{\pi\omega^2(z)} exp(-2\left[\frac{x^2+y^2}{\omega^2(z)}\right])} \quad (9)$$

where $x.y.z$ are the Cartesian coordinates, P_0 is the laser beam power, $\omega(z)$ is the beam radius at the height of z and it is assumed to be linear.

Laser energy attenuation is calculated due to the Beer-Lambert equation[32]:

$$\boldsymbol{I_{attenuated} = I_0 exp\left(-\sigma_{ext} N_p \Delta z\right)} \quad (10)$$

where I_0 is the energy intensity before being attenuated in a powder stream, Δz is the length that beam passes through powder stream, N_p is particle concentration of the volume element. σ_{ext} represents the extinction cross section of a particle given by $\sigma_{ext} = Q_{ext}\pi r^2$ and Q_{ext} is the extinction coefficient. As the particle size is much bigger than the laser wavelength in the LDED process, it could be assumed that the

extinction coefficient $Q_{ext} = 1$ and the extinction cross section equals to cross section of the particle [14, 18, 42].

To consider the Gaussian distribution and also beam divergence in determining I_0 in Eq. (10), the laser beam has been split radially into truncated cones as shown in Fig. 6.

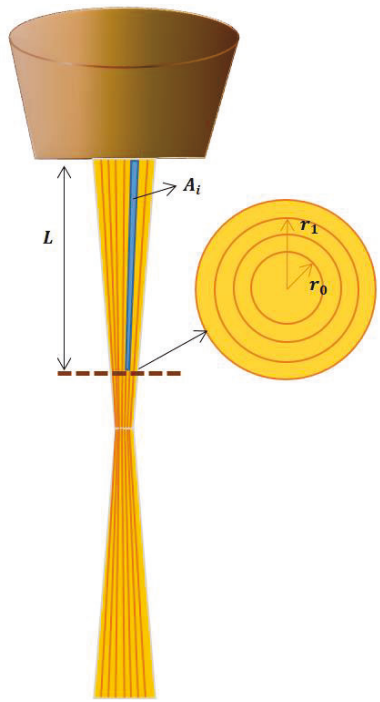

Fig. 6 Splitting of the laser beam for considering laser intensity distribution in attenuation calculation

As it is shown in Fig. 6, any plane perpendicular to the laser beam axis, is divided into some concentrated rings. The attenuated laser energy distribution can be obtained from the attenuated energy on these rings. To calculate attenuated laser energy on each ring, a fixed amount of energy intensity could be assigned to the beam reaching the ring by following equation:

$$\boldsymbol{I_i} = \frac{\left[\int_{r0}^{r1}\int_0^L \frac{2P_0}{\pi\omega^2(z)} exp\left(-2\left[\frac{r^2}{\omega^2(z)}\right]dzdr\right)\right]}{A_i} \tag{11}$$

where I_i is energy intensity reaching the ith ring (I_0 in Eq. (10)), L is the height of the plane on which the laser energy distribution is being calculated, r_0 and r_1 are the

inner and outer radius of the ring and A_i is the area of the trapezius plane with $(r_1 - r_0)$ and L as its sides. It is worth mentioning that as the laser beam is axisymmetric it is no need for integrating on rotational direction.

In most of the studies, powder distribution is considered as Gaussian, however, the assumption of the standard Gaussian model may not always be accurate, since it may deviate from Gaussian depending on powder properties, configurations of nozzle, gas settings, and standoff distances [43] .Therefore, in this study, instead of considering a predefined pattern for powder distribution, the powder stream distribution is derived from the 3D model of powder stream. As shown schematically in Fig. 7, the powder particles in each partition of the split laser beam could be defined from the output of the 3D model of gas-powder flow.

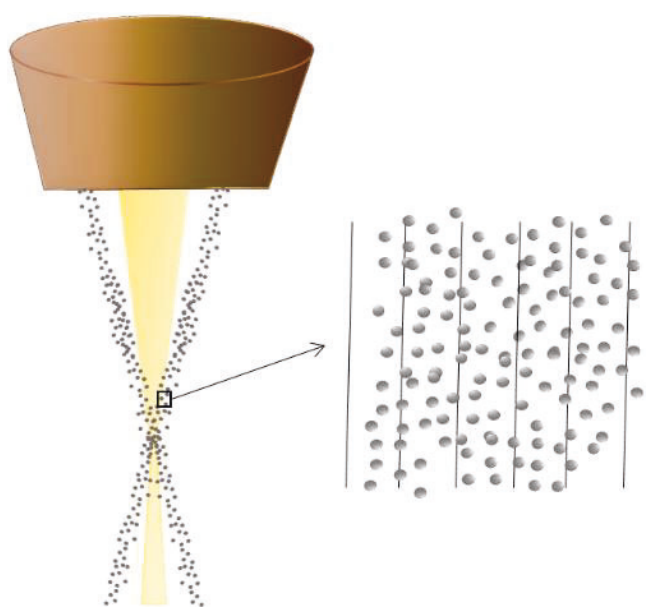

Fig. 7 schematic of defining the powder particles in each partition of the laser beam from the 3D model of powder stream

3.1MATLAB GUI

A GUI has been created in MATLAB to calculate laser attenuation for any configuration of the laser beam, powder stream distribution, and workpiece distance

from the nozzle head. The GUI is shown in Fig. 8. It gets laser properties and powder distribution profile and uses equations (9) to (10) to calculate laser attenuation on any ring on the workpiece surface, made by a split laser beam. And at the end, the output of the program would be a plot of attenuated laser intensity distribution on the workpiece and also the original laser intensity for comparison.

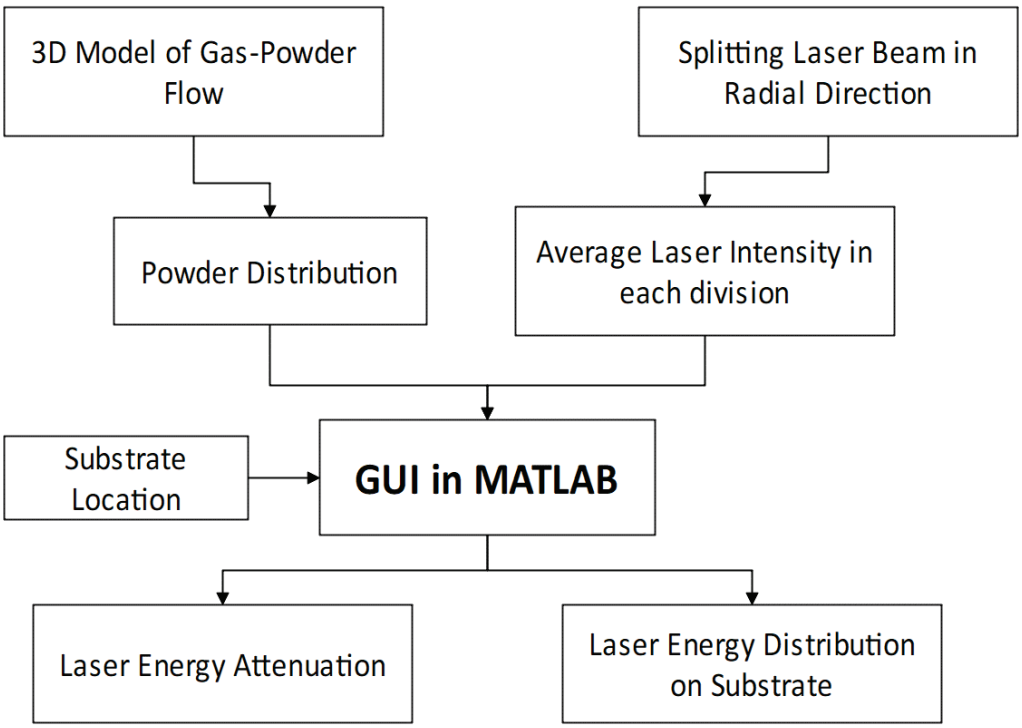

Fig. 8 GUI created in MATLAB for calculating laser attenuation in the LDED process

4. Results and discussion

The laser attenuation calculation was carried out on a laser with properties similar to Moradi [40, 41] experimental study. The laser beam profile is assumed as Gaussian with power of 400W. The laser beam radius at nozzle head position is 0.35 mm and the minimum focal spot size is of 0.2 mm. The focal plane position of the laser can be placed between 14 and 17 mm below the nozzle head.

For modeling the gas-powder flow, the carrier gas and shielding gas flow was set to 6 lit/min and 3 lit/min and powder density was considered to be 8 gr/cm^3.

The effect of powder mass flow rate, powder size, workpiece distance from nozzle head on laser attenuation, and its intensity distribution was investigated in this study.

4.1Powder mass flow rate

To survey the influence of powder mass flow rate on laser attenuation, the calculation was applied on the result of the 3D model for the powder flow rate of 0.04, 0.08, 0.12, and 0.15 gr/s and particles with a constant diameter of 70 µm. It was assumed that the workpiece and laser focal plane are at the same position as the powder flow concentration plane at 15 mm below the nozzle head. The attenuated laser energy distribution on the workpiece in comparison to its original amounts is shown in Fig. 9.

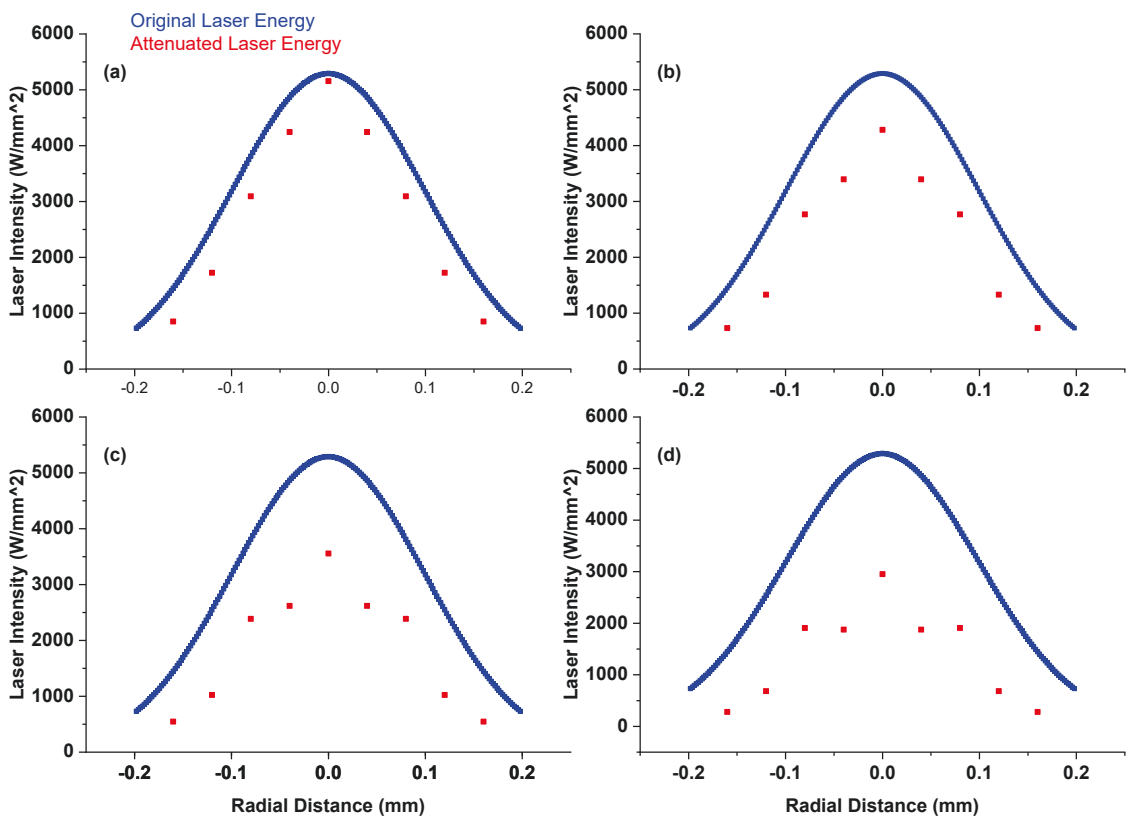

Fig. 9 Laser intensity distribution on the workpiece surface for powder flow rate of (a) 0.04 gr/s, (b) 0.08 gr/s, (c) 0.12 gr/s and (d) 0.15 gr/s

The average attenuation of laser energy for different powder mass flow rates can be seen in the diagram of Fig. 10.

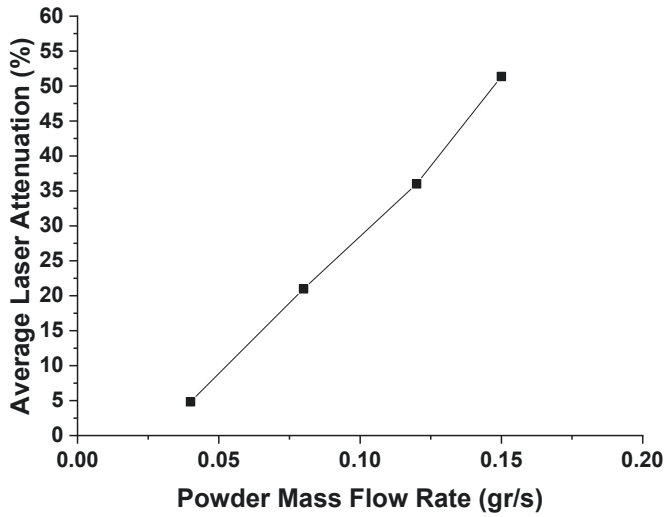

Fig. 10 Average attenuation percent via powder mass flow rates.

As it is shown in Fig. 9 and Fig. 10, an increase in powder mass flow rate would increase the energy attenuation almost linearly. It is due to more powder particles being in the way of the laser beam to absorb its energy.

4.2 Powder size

Another parameter that affects the energy amount and distribution on the workpiece surface is powder particles size. To understand this effect, the GUI was run for the result of the 3D model for a particle diameter of 20, 50, 70, and 100 μm and a constant mass flow rate of 0.08 gr/s. It was assumed that the workpiece and laser focal plane are at the same position as the powder flow concentration plane at 15 mm below the nozzle head. The attenuated laser energy distribution on the workpiece in comparison to its original amounts is shown in Fig. 11. As it can be seen, laser intensity distribution on the workpiece surface differs from its original Gaussian shape. It is the result of powder distribution pattern which is affected by particle size as is illustrated in Fig. 12. Since smaller particles are lighter than bigger ones, they are more affected by the central shielding gas, and they are blown off from the central axis more. And also the weight of the particles is one of the parameters that defines their trajectories. So as the particle diameter decreases, the

powder stream structure deviates from Gaussian shape more and causes the attenuated laser intensity distribution also deviates from its original Gaussian profile.

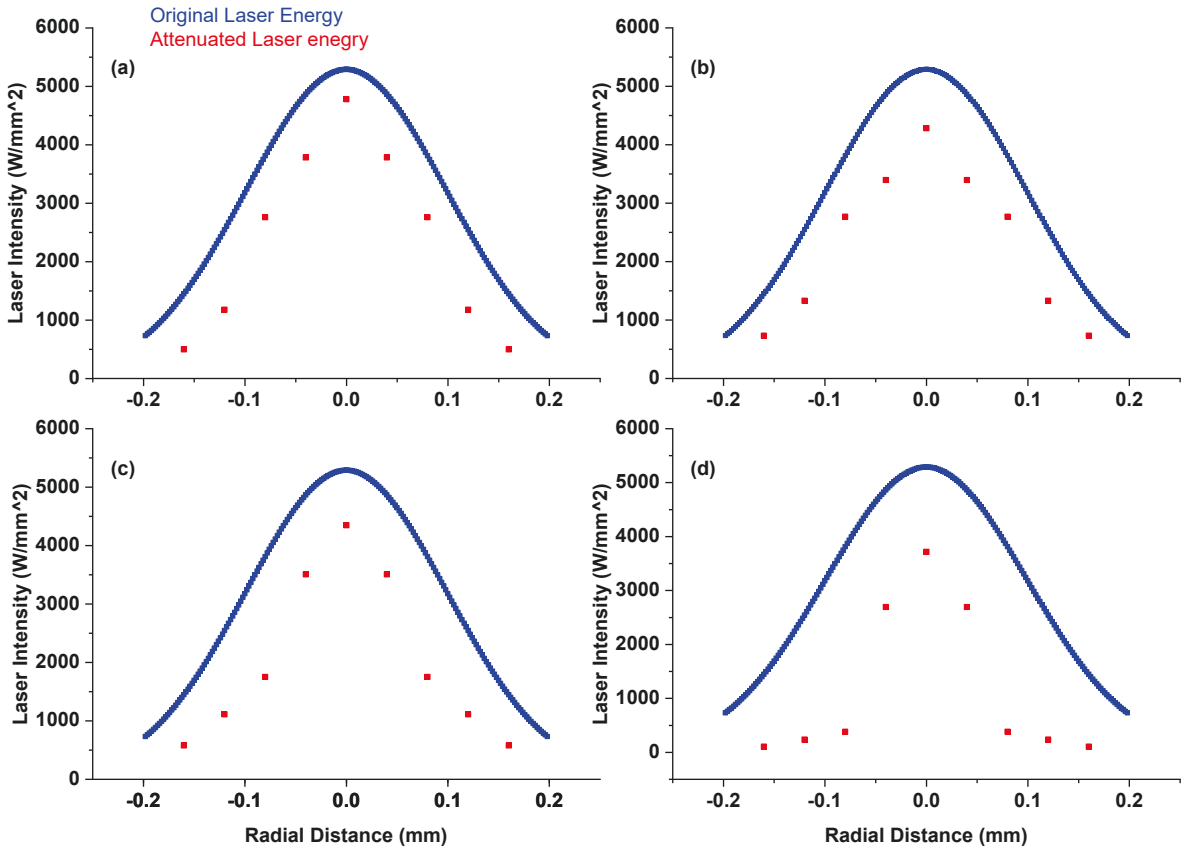

Fig. 11. Laser intensity distribution on the workpiece surface for a particle diameter of (a) 100 µm, (b) 70 µm, (c) 50 µm (d) 20 µm

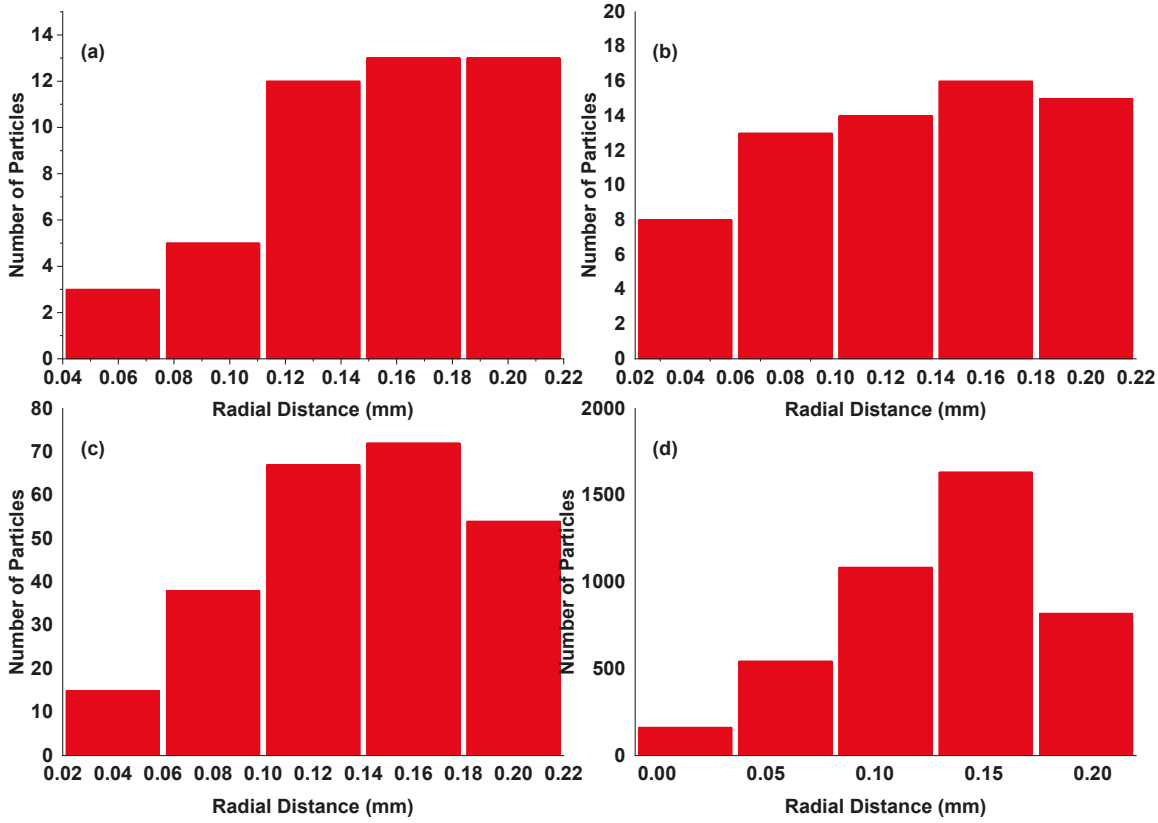

Fig. 12 Powder distribution in laser powder stream interaction zone

The average attenuation of laser energy for different powder sizes can be seen in the diagram of Fig. 13.

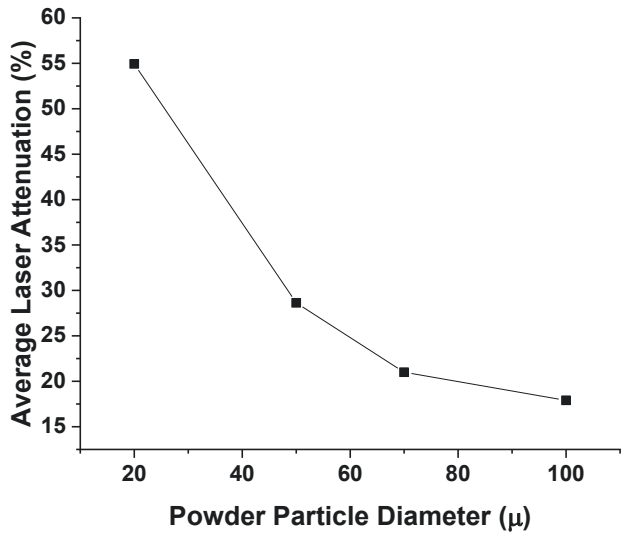

Fig. 13 Average attenuation percent via powder particle diameter.

It can be seen that the attenuation increases as the particles become smaller.

For a constant mass flow rate, a decrease in diameter leads to an increase in particle numbers by an order of three (Eq. (12)). Furthermore, as illustrated in Eq. (10), the diameter of the particle appears in this equation by order of two and the number of particles affects the equation by order of one. Thus, the exponential term in this equation grows as the diameter increase and the minus sign of the exponential term eventually results in larger attenuation. Therefore, the nonlinear increase in attenuation by a decrease in powder particle diameter could be seen in Eq. (12).

$$\dot{m}_{powder} = \dot{n}_{particles} \times \rho_{powder} \times \left(\frac{4}{3}\pi\left(\frac{Diameter_{particles}}{2}\right)^3\right) \quad (12)$$

4.3Workpiece position

As it was discussed before, the laser beam is not a constant radius cylinder and its radius varies in the longitudinal direction, so where the workpiece is placed would define the laser beam radius at the workpiece surface. The position of the workpiece would also affect the number of particles that interact with the laser beam on their way to the melt pool[10, 44]. However, to understand the effect of workpiece

position on the laser energy and its distribution, the GUI was run for powder stream with a constant mass flow rate of 0.08 gr/s, the constant particle diameter of 70 µm, and for 4 different positions of the workpiece as shown in Fig. 14. The focal plane of the laser was set on a powder stream concentration plane 15 mm below the nozzle head.

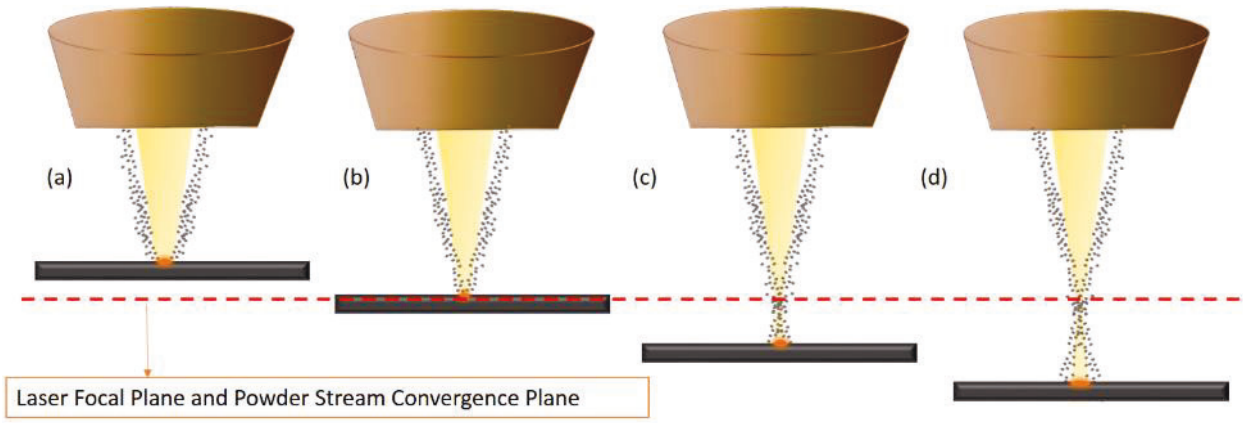

Fig. 14 Workpiece location, (a) 14 mm, (b) 15 mm, (c) 16 mm (d) 20 mm below nozzle head.

The attenuated laser energy distribution on the workpiece in comparison to its original amounts is shown in Fig. 15.

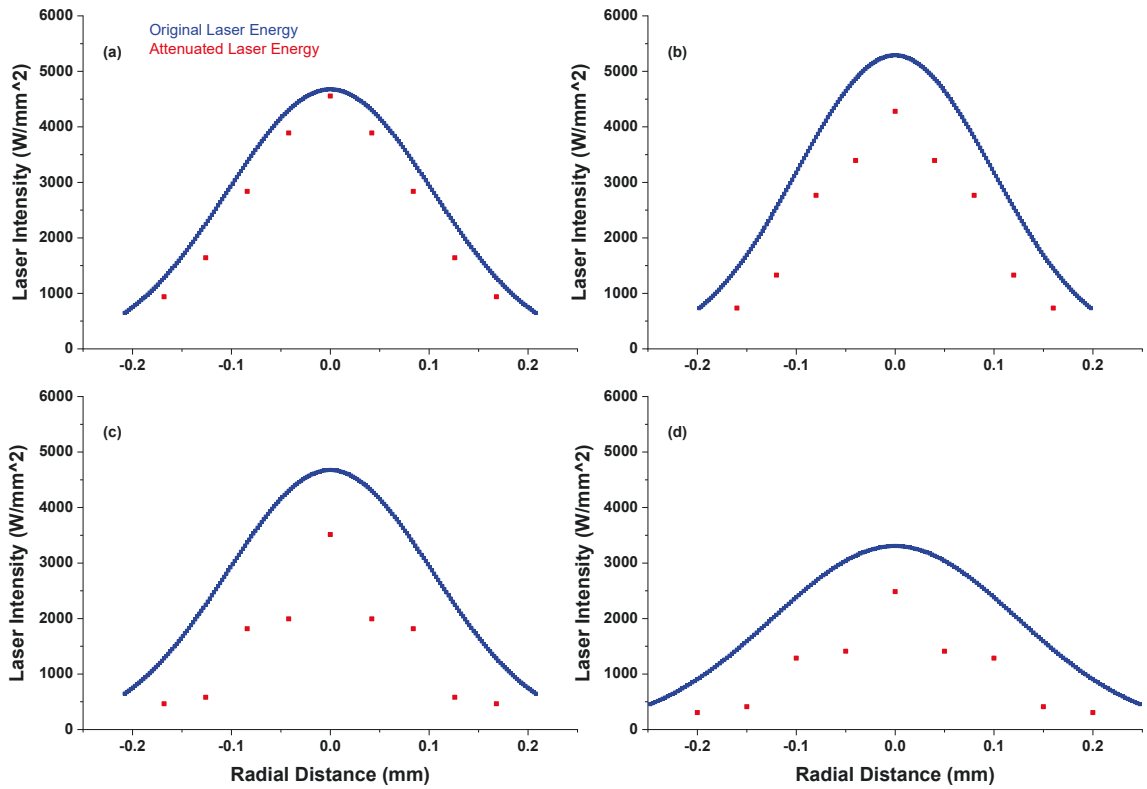

Fig. 15 Laser intensity distribution on the workpiece surface for workpiece placed (a) 14 mm, (b) 15 mm, (c) 16 mm (d) 17 mm below nozzle head

The average attenuation of laser energy for different powder sizes can be seen in the diagram of Fig. 16 .

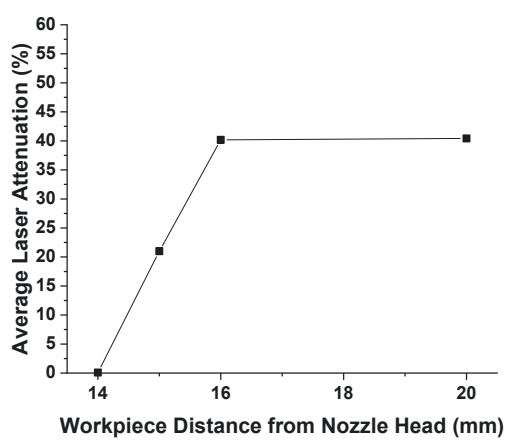

Fig. 16 Average attenuation percent via workpiece distance from nozzle head.

It can be concluded from Fig. 15 and Fig. 16 that when the workpiece is above the powder stream convergence plane and laser focal plane, the attenuation would be trivial. The four powder streams have not crossed each other yet and they are on the perimeter of a circle with a larger radius than the laser beam radius and melt pool dimensions. Therefore, there are few numbers of powder particles interacting with the laser beam and dropping into the melt pool. It should be considered that in this case, the powder catchment and so the process efficiency would also be very low. Moreover, the maximum laser intensity on any plane would be smaller than the maximum intensity on the focal plane due to the minimum laser spot on the focal plane. Another conclusion to be noted is that by increasing the workpiece distance from the laser focal plane and powder stream consolidation plane, Figure 11-d, attenuation remains almost constant. This is because powder streams start to diverge after the consolidation plane, hence, they lost their interaction with the laser beam. However, when the workpiece is placed farther from the concentration plane, the radius of the powder stream gets larger and consequently the number of particles dropping in the melt pool decreases, and the powder catchment declines.

5. Conclusion

In the present study, laser energy intensity on the workpiece surface, in the LDED process is figured by considering laser attenuation. The attenuation was calculated without common simplification on laser beam shape and powder stream structure. The laser beam divergence angle is taken into account and powder distribution is defined from a 3D model of gas-powder flow. The effect of powder mass flow rate, powder size, and workpiece position on laser attenuation is studied, and the results are as follow:

- For constant powder size, an increase in mass flow rate would increase laser attenuation almost linearly due to the presence of more powder particles in the way of the laser beam to extinct its energy.
- Powder particle size has an influence on powder stream distribution in laser and powder stream interaction zone, so the laser attenuation and consequently laser intensity distribution on the workpiece surface would be affected by powder size.
- For constant mass flow rate, smaller powder particles attenuate laser energy more than bigger ones, as it was shown in section 4.2, for a constant mass flow rate decreasing powder size from 100 μ to 20 μ, increases attenuation from 18% up to 55%.
- If the workpiece places above the laser focal plane and powder stream concentration plane, the attenuation is almost zero, but it is not a good setup for the process due to low powder catchment.
- When the workpiece is below the laser focal plane and powder stream concentration plane, the distance does not affect the laser attenuation since the number of powders in the interaction zone of laser and powder stream is constant as the powder stream diverges after the convergence plane, and they don't have interaction with laser beam anymore.
- If the workpiece locates on the laser focal plane, the workpiece surface would experience the maximum laser energy intensity due to the smallest spot size of the laser beam on this plane.

Conflicts of interest/Competing interests:

The authors declared no potential conflicts of interest/competing interests with respect to the research, authorship, and/or publication of this article.

Funding:

No funds, grants, or other support was received.

Authors' contributions:

Niloufar Sobhanieh: Conceptualization, Methodology, Resources, Writing-Original Draft. (First author).

Javad Akbari: Supervision and Editing. (Corresponding author).

Mahmoud Moradi: Supervision and Editing.

Consent to Participate:

The authors agreed to participate in this manuscript.

Consent to Publish:

The authors agreed with this submission.

Ethical Approval:

Our paper is an original paper which has neither previously, nor simultaneously, in whole or in part been submitted anywhere else. All authors prove that the paper is an original paper.

Availability of data and materials:

All data generated or analyzed during this study are included in this published article.

6. References

1. Moradi, M., Hasani Arman, Pourmand Zeynab, Lawrence Jonathan, *Direct laser metal deposition additive manufacturing of Inconel 718 superalloy: Statistical modelling and optimization by design of experiments.* Optics & Laser Technology, 2021. **144**: p. 107380.
2. Pinkerton, A.J. and L. Li, *Modelling powder concentration distribution from a coaxial deposition nozzle for laser-based rapid tooling.* J. Manuf. Sci. Eng., 2004. **126**(1): p. 33-41.
3. Lednev, V.N., P.A. Sdvizhenskii, R.D. Asyutin, R.S. Tretyakov, M.Y. Grishin, A.Y. Stavertiy, A.N. Fedorov and S.M. Pershin, *In situ elemental analysis and failures detection during additive manufacturing process utilizing laser induced breakdown spectroscopy.* Opt Express, 2019. **27**(4): p. 4612-4628.
4. Martin, J.H., B.D. Yahata, J.M. Hundley, J.A. Mayer, T.A. Schaedler and T.M. Pollock, *3D printing of high-strength aluminium alloys.* Nature, 2017. **549**(7672): p. 365-369.
5. DebRoy, T., T. Mukherjee, H. Wei, J. Elmer and J. Milewski, *Metallurgy, mechanistic models and machine learning in metal printing.* Nature Reviews Materials, 2021. **6**(1): p. 48-68.
6. Khairallah, S.A., A.A. Martin, J.R. Lee, G. Guss, N.P. Calta, J.A. Hammons, M.H. Nielsen, K. Chaput, E. Schwalbach and M.N. Shah, *Controlling interdependent meso-nanosecond dynamics and defect generation in metal 3D printing.* Science, 2020. **368**(6491): p. 660-665.
7. Liu, D.-R., S. Wang and W. Yan, *Grain structure evolution in transition-mode melting in direct energy deposition.* Materials & Design, 2020. **194**: p. 108919.
8. Liu, F., L. Wei, S. Shi and H. Wei, *On the varieties of build features during multi-layer laser directed energy deposition.* Additive Manufacturing, 2020. **36**: p. 101491.
9. Wu, J., P. Zhao, H. Wei, Q. Lin and Y. Zhang, *Development of powder distribution model of discontinuous coaxial powder stream in laser direct metal deposition.* Powder Technology, 2018. **340**: p. 449-458.
10. Liu, C.-Y. and J. Lin, *Thermal processes of a powder particle in coaxial laser cladding.* Optics & Laser Technology, 2003. **35**(2): p. 81-86.
11. Wirth, F., S. Freihse, D. Eisenbarth and K. Wegener. *Interaction of powder jet and laser beam in blown powder laser deposition processes: Measurement and simulation methods*. in *Lasers in Manufacturing Conference, Munich, Germany*. 2017.
12. Lia, F., J. Park, J. Tressler and R. Martukanitz, *Partitioning of laser energy during directed energy deposition.* Additive Manufacturing, 2017. **18**: p. 31-39.
13. Wang, Z., T.A. Palmer and A.M. Beese, *Effect of processing parameters on microstructure and tensile properties of austenitic stainless steel 304L made by directed energy deposition additive manufacturing.* Acta Materialia, 2016. **110**: p. 226-235.
14. Huang, Y., M.B. Khamesee and E. Toyserkani, *A comprehensive analytical model for laser powder-fed additive manufacturing.* Additive Manufacturing, 2016. **12**: p. 90-99.
15. Xiong, Y., J.E. Smugeresky and J.M. Schoenung, *The influence of working distance on laser deposited WC–Co.* Journal of Materials Processing Technology, 2009. **209**(10): p. 4935-4941.

16. De Oliveira, U., V. Ocelik and J.T.M. De Hosson, *Analysis of coaxial laser cladding processing conditions.* Surface and Coatings Technology, 2005. **197**(2-3): p. 127-136.
17. Kistler, N.A., A.R. Nassar, E.W. Reutzel, D.J. Corbin and A.M. Beese, *Effect of directed energy deposition processing parameters on laser deposited Inconel® 718: Microstructure, fusion zone morphology, and hardness.* Journal of Laser Applications, 2017. **29**(2): p. 022005.
18. Han, L., K. Phatak and F. Liou, *Modeling of laser cladding with powder injection.* Metallurgical Materials transactions, 2004. **35**(6): p. 1139-1150.
19. Balu, P., P. Leggett and R. Kovacevic, *Parametric study on a coaxial multi-material powder flow in laser-based powder deposition process.* Journal of Materials Processing Technology, 2012. **212**(7): p. 1598-1610.
20. Thompson, S.M., L. Bian, N. Shamsaei and A. Yadollahi, *An overview of Direct Laser Deposition for additive manufacturing; Part I: Transport phenomena, modeling and diagnostics.* Additive Manufacturing, 2015. **8**: p. 36-62.
21. Lin, J., *Laser attenuation of the focused powder streams in coaxial laser cladding.* Journal of laser applications, 2000. **12**(1): p. 28-33.
22. Guan, X. and Y.F. Zhao, *Numerical modeling of coaxial powder stream in laser-powder-based Directed Energy Deposition process.* Additive Manufacturing, 2020. **34**: p. 101226.
23. Tamanna, N., R. Crouch and S. Naher, *Progress in numerical simulation of the laser cladding process.* Optics and Lasers in Engineering, 2019. **122**: p. 151-163.
24. Zhang, Z., P. Ge, T. Li, L.-E. Lindgren, W. Liu, G. Zhao and X. Guo, *Electromagnetic wave-based analysis of laser–particle interactions in directed energy deposition additive manufacturing.* Additive Manufacturing, 2020. **34**: p. 101284.
25. Liu, Z., H.-C. Zhang, S. Peng, H. Kim, D. Du and W. Cong, *Analytical modeling and experimental validation of powder stream distribution during direct energy deposition.* Additive Manufacturing, 2019. **30**: p. 100848.
26. Yao, X., J. Li, Y. Wang, X. Gao, T. Li and Z. Zhang, *Experimental and numerical studies of nozzle effect on powder flow behaviors in directed energy deposition additive manufacturing.* International Journal of Mechanical Sciences, 2021. **210**: p. 106740.
27. Kovalev, O., I. Kovaleva and I.Y. Smurov, *Numerical investigation of gas-disperse jet flows created by coaxial nozzles during the laser direct material deposition.* Journal of Materials Processing Technology, 2017. **249**: p. 118-127.
28. Diniz Neto, O. and R. Vilar, *Physical–computational model to describe the interaction between a laser beam and a powder jet in laser surface processing.* Journal of Laser Applications, 2002. **14**(1): p. 46-51.
29. Diniz Neto, O., A. Alcalde and R. Vilar, *Interaction of a focused laser beam and a coaxial powder jet in laser surface processing.* Journal of Laser Applications, 2007. **19**(2): p. 84-88.
30. Pinkerton, A.J., *An analytical model of beam attenuation and powder heating during coaxial laser direct metal deposition.* Journal of Physics D: Applied Physics, 2007. **40**(23): p. 7323.
31. Tabernero, I., A. Lamikiz, S. Martinez, E. Ukar and L.L. De Lacalle, *Modelling of energy attenuation due to powder flow-laser beam interaction during laser cladding process.* Journal of materials processing technology, 2012. **212**(2): p. 516-522.

32. Jiazhu, W., T. Liu, H. Chen, F. Li, H. Wei and Y. Zhang, *Simulation of laser attenuation and heat transport during direct metal deposition considering beam profile.* Journal of Materials Processing Technology, 2019. **270**: p. 92-105.
33. Devesse, W., D. De Baere and P. Guillaume, *Modeling of laser beam and powder flow interaction in laser cladding using ray-tracing.* Journal of Laser Applications, 2015. **27**(S2): p. S29208.
34. Li, W., J. Zhang, S. Karnati, Y. Zhang, F. Liou, J. Newkirk and K.M. Brown Taminger. *Modeling and Experimental Investigation of Pre-Mixed Multi-Powder Flow in Fabricating Functional Gradient Material by Laser Metal Deposition Process*. in *Proceedings of the 27th Solid Freeform Fabrication Symposium (2016, Austin, TX)*. 2016.
35. Zekovic, S., R. Dwivedi and R. Kovacevic, *Numerical simulation and experimental investigation of gas–powder flow from radially symmetrical nozzles in laser-based direct metal deposition.* International Journal of Machine Tools and Manufacture, 2007. **47**(1): p. 112-123.
36. Morville, S., M. Carin, D. Carron, P. Le Masson, M. Gharbi, P. Peyre and R. Fabbro. *Numerical modeling of powder flow during coaxial laser direct metal deposition–comparison between Ti-6Al-4V alloy and stainless steel 316L*. in *Proceedings of the 2012 COMSOL Conference, Milan*. 2012.
37. Li, W., X. Zhang and F. Liou, *Modeling analysis of argon gas flow rate's effect on pre-mixed powder separation in laser metal deposition process and experimental validation.* The International Journal of Advanced Manufacturing Technology, 2018: p. 1-11.
38. Launder, B.E. and D.B. Spalding, *Lectures in mathematical models of turbulence.* 1972.
39. Guide, A.F.U., *Release 14.0, ANSYS.* Inc., USA, November, 2011.
40. Moradi, M., A. Ashoori and A. Hasani, *Additive manufacturing of stellite 6 superalloy by direct laser metal deposition–Part 1: Effects of laser power and focal plane position.* Optics & Laser Technology, 2020. **131**: p. 106328.
41. Moradi, M., A. Hasani, Z.M. Beiranvand and A. Ashoori, *Additive manufacturing of stellite 6 superalloy by direct laser metal deposition–Part 2: Effects of scanning pattern and laser power reduction in differrent layers.* Optics & Laser Technology, 2020. **131**: p. 106455.
42. Frenk, A., M. Vandyoussefi, J.-D. Wagniere, W. Kurz and A. Zryd, *Analysis of the laser-cladding process for stellite on steel.* Metallurgical and Materials transactions B, 1997. **28**(3): p. 501-508.
43. Wen, S., Y. Shin, J. Murthy and P. Sojka, *Modeling of coaxial powder flow for the laser direct deposition process.* International Journal of Heat Mass Transfer, 2009. **52**(25-26): p. 5867-5877.
44. Haley, J.C., B. Zheng, U.S. Bertoli, A.D. Dupuy, J.M. Schoenung and E.J. Lavernia, *Working distance passive stability in laser directed energy deposition additive manufacturing.* Materials & Design, 2019. **161**: p. 86-94.